Automatic prediction of isocitrate dehydrogenase mutation status of low-grade gliomas using radiomics and domain knowledge inspired features in magnetic resonance imaging

Düşük evreli gliomların radiomic ve alan bilgisi temelli öznitelikler aracılığı ile manyetik rezonans görüntülerinden izositrat dehidrogenaz mutasyon durumunun otomatik tahmini

Ilker Ozgür Koska[1], Cagan Koska[2], Antonio Fernandes[3]

[1] Division of Radiology, İzmir Behçet Uz Training and Research Hospital

[2] Private İlgi Science High School

[3] Sliced Group

Abstract

Aim: Most common and most deadly primary central nervous tumors, glial tumors harbor many heterogeneous clones of cells. Noninvasive determination of the genomic profiles of these tumors would have important implications regarding the classification, management, and prognostication of these tumors. Isocitrate dehydrogenase mutation is a key genomic signature that can downgrade the expected dismal course of these tumors. In this study we aimed to build a performant prediction model which can determine the Isocitrate Dehydrogenase (IDH) mutation status of glial tumors, using radiomics and leveraging automatic computation of domain knowledge-inspired features.

Methods: Radiomics methods based on high throughput feature extraction and application of data science principles to these extracted features are promising tools for the noninvasive classification of lesions. Domain knowledge-inspired features besides radiomics features can contribute positively to the performance of the models. Some efforts particularly a joint approach to standardize the magnetic resonance imaging (MRI), reporting of glial tumors are mainstay for domain knowledge-inspired features. However, this requires active involvement and reporting of the radiologist which hampers automatization efforts. Additionally, this feature set evaluates a small subset of all possible signal and spatial-based computations. In this study, we combined domain knowledge-inspired features with radiomics features along with a multiparametric multihabitat comprehensive lesion description strategy.

Results: Our best model which consisted of a combination of radiomics, and radiologist knowledge-inspired features reached a 0.93 f1 score (standard deviation (SD): 0.03), 0.93 accuracy (SD:0.03), and 0.98 area under curve (AUC), (SD:0.02).

Conclusion: The multiparametric and multiregional approach employed in this study coupled with the integration of both radiomics and domain knowledge-inspired features resulted in a high-performance model emphasizing the contribution of each strategy to the outcome.

Keywords: Glial cell tumors; mutation; radiomics

Öz

Amaç: En yaygın ve en ölümcül birincil merkezi sinir tümörleri olan glial tümörler, heterojen hücre klonları barındırırlar. Glial tümörlerin genomik profillerinin invazif olmayan bir şekilde belirlenmesi, bu tümörlerin sınıflandırılması, yönetimi ve prognostikasyonu ile ilgili önemli etkilere sahip olacaktır. İzositrat dehidrogenaz mutasyonu varlığı bu tümörler için önemli bir genetik belirteç olup daha iyi prognoz göstergesidir. Radyomik yöntemler, lezyonların non invazif sınıflandırılması için umut verici bir araçtır. Bu çalışmada radyomik özelliklerin yanı sıra alan bilgisinden ilham alan özelliklerle, yapay zekâ ile manyetik rezonans görüntüleme (MRI), görüntülerinden İzositrat Dehidrogenaz (IDH) mutasyon tahmini yapacak bir model geliştirilmesi amaçlanmıştır.

Yöntemler: Radyomik öznitelik kümesi çıkarılmış buna ek olarak radyologların lezyon tariflemede kullandığı belirteçler kodlanarak otomatik olarak elde edilmeye çalışılmıştır. Her iki yöntem ile elde edilen öznitelikler ile sınıflayıcı modeler geliştirilmiştir.

Bulgular: Radyomik ve radyolog bilgisinden ilham alan özelliklerin kombinasyonundan oluşan en iyi modelimiz 0,93 f1 puanı (Standart Sapma (SD): 0,03), 0,93 doğruluk (SD:0,03) ve 0,98 eğri altındaki alan (EAA)'ya (SD:0,02) ulaştı.

Sonuç: Bu çalışmada kullanılan çok parametreli ve çok bölgeli yaklaşım hem radyomik hem de alan bilgisinden ilham alan özelliklerin entegrasyonu ile birleştiğinde, nihai sonuç için her bir stratejinin katkısını vurgulayan yüksek performanslı bir modelle sonuçlandı.

Anahtar Sözcükler: Glial hücreli tümörler; mutasyon; yapay zeka

Received/*Geliş* : 24.10.2023
Accepted/*Kabul*: 31.12.2023

DOI: 10.21673/anadoluklin.1378673

Corresponding author/*Yazışma yazarı*

İlker Özgür Koska
İzmir Behçet Uz Eğitim Araştırma Hastanesi, Radyoloji Bölümü, İzmir, Türkiye.
E-mail: ozgurkoska@yahoo.com

ORCID
İlker Özgür Koska: 0000-0003-0971-3827
Çağan Koska: 0000-0003-0484-5046
Antonio Fernandes: 0000-0002-0446-4422

INTRODUCTION

Glial tumors are the most common primary malign neoplasms of the central nervous system (1). The presence of isocitrate dehydrogenase (IDH1) mutation which involves arginine in position 132 may be seen in 50-80 % of low-grade glioma (LGG) and 12% of high-grade glioma (HGG) (2,3). IDH mutation may render the glial tumors into a less aggressive type which exhibits significantly higher survival times regardless of histological grade (2,4). Its critical role in prognostication leads to its inclusion in World Health Organisation (WHO) 2016 and 2021 glial tumor classification criteria (5,6). The glial tumors are subdivided into four grades according to WHO classification. Significant survival differences appear on the same grade based on IDH mutation presence or absence (7). IDH enzyme takes place in oxygenated respiration of cell metabolism. In the wild form, the cell normally converts isocitrate into alpha-ketoglutarate in the Krebs cycle while in the mutated form conversion is driven to 2-hydroxyglutarate which inhibits downstream histone demethylases (8). Current state-of-the-art IDH mutation detection is based on immunohistochemical staining or genetic profiling which requires surgical or interventional tissue sampling. However spatial and spectral heterogeneity of tumors may sometimes result in over or underestimation of genomic status of the tumor (9,10).

Identification of the IDH status of glial tumors can help clinicians in several aspects. LGG with IDH mutation can be subject to and see approach. Additionally, IDH mutant cells have increased sensitivity to chemotherapy and radiotherapy which can determine the choice of treatment (11). Therefore, non-invasive determination of IDH status is an important and unsolved problem in the literature. Some studies use conventional imaging features, Visually Accessible Rembrandt Images (VASARI) features, radiomics, and deep learning to propose solutions to this problem (12-15). Conventional imaging features and VASARI features are based on the knowledge of human radiologists. The former approach depends on the vectorization of the imaging clues for further utilization of statistical methods and the latter is based on scoring standardized properties of a tumor including location, various proportions of different habitats of the tumor, and certain imaging features (16). These approaches are limited to large-scale analysis of images which can roughly reflect underlying molecular and cellular characteristics. However human eye is not sensitive to the above second-order relationship of individual image components (17). Deep learning studies based on imaging features require many images to automatically find relevant features in the images. However, in medical imaging, image resources are limited due to strict regulations of sensitive data. Radiomics which can be interpreted as digital biopsy is based on its central dogma which states that images are reflections of underlying molecular, cellular, and metabolic processes and they can be represented by various computational tools (18). Recently radiomics methods have been used to analyze various Computer Tomography (CT) and Magnetic Resonance Imaging (MRI) classification tasks successfully (19-22). We hypothesized that different MRI sequences and different habitats in these sequences may harbor complementary information regarding the explanation of underlying biology.

In this study, our aim was to explore the multiparametric multihabitat radiomics methods to build a robust classifier model that can successfully determine the IDH status of glial tumors in MR images.

MATERIAL AND METHODS

Patients

We obtained genetic and MR imaging low-grade glioma (LGG) data from the Cancer Imaging Archive (23). The ethical board approval of the data was handled by the providers of this publicly available repository. Therefore, we did not obtain additional ethical board approval and informed patient consent since this kind of data is exempt from additional ethical board approval and consent requirements. The MR image data sets were downloaded from the Cancer Imaging Archive in July 2022 (www.cancerimagingarchive.net) and originated from five centers (Thomas Jefferson University, Philadelphia, MD, Henry Ford Hospital, Detroit, MI, Saint Joseph Hospital and Medical Center, Phoenix, AZ, Case Western Reserve University, Cleveland, OH and University of North Carolina, Chapel Hill, NC).

The inclusion criteria for this study were presurgical axial T1, contrast-enhanced T1 (T1CE), T2 and Fluid Attenuated Inversion Recovery (FLAIR) images, and treatment-naive gene expression data (Figure 1). We included 108 patients who had readily available annotation masks for tumor necrotic zone, enhancing tumor and peritumoral edema regions. 7 patients were additionally excluded since they did not have data indicating their IDH status. All the analyses were held on the remaining 101 patients (Figure 2).

Preprocessing:

These scans were initially skull-stripped and co-registered to SR124 atlas, before their tumor segmentation labels were produced by an automated hybrid generative-discriminative method, ranked first during the International Multimodal Brain Tumor Segmentation Challenge (BRATS 2015) (23). These segmentation labels were revised, and any label misclassifications were manually corrected by an expert board-certified neuroradiologist (23). Images were resampled into 1mm resolution and signal intensity was normalized to the 0-1 range. Sample MRI images from both classes were provided in Figure 1.

Feature Extraction:

Two different feature extraction strategies were employed. One was radiomics with a radionics package and the other one was the automatization of a radiologist decision-making process inspired by VASARI features (16).

Pyradiomics (18) an open-source Python package (v3.0 https://pyradiomics.readthedocs.io/en/latest/) was used for feature extraction. Voxels were resampled into 1x1x1 mm resolution by a cubic b-spline algorithm to correct acquisition-related variations and discretized into a bin width of 25 followed by normalization with the normalized scale of 300. Laplacian of Gaussian (LoG) filter transformation with 5 distinct sigma values and one level 3D wavelet transformation was used along with original images yielding 1218 features. The same strategy was applied for 3 sequences (T1CE, T2, and FLAIR) and 2 habitats (tumor core and whole tumor). There were 4 possible sequences including T1 and 7 possible tissue types (necrosis, enhancing tumor, tumor core which consists of the former two, edema, whole tumor, edema plus enhancing tumor, and normal appearing peritumoral brain region). This would yield 7x4x1218 = 34104 features. After initial exploration we decided to proceed with 2 tissue types (tumor core and whole tumor) and 3 different MRI sequences) which produced a better feature set. This approach effectively reduced the number of features to 3X2X1218= 7308. Then we applied unsupervised feature selection to decrease the number of features. First, we eliminated the features with less than 5% variance. Because the additional contribution of these to the model would be limited. Then we eliminated the features with a correlation coefficient higher than 0.8. Since the information they would provide would be similar, their contribution would be low, on the contrary, they would complicate the model's performance due to multicollinearity.

For the second feature extraction approach we calculated the signal and spatial properties of the images. For spatial features, the volumes of each tissue type (necrosis, enhancing tumor, tumor core, edema, and whole tumor) were calculated and compared with each other. Thus, 20 different ratios (5x4) were obtained by the permutations of volumes of 5 tissue types. In MR, the signal properties are affected by the imaging parameters and the equipment used, as well as the tissue type displayed. For this reason, using the absolute value of the signal may give misleading results due to the images obtained on different machines. However, proportioning the signals in different sequences or different tissue regions in the same sequence to each other can eliminate this problem by creating an internal normalization. For this reason, we calculated the mean, minimum, maximum, and standard deviation values of the signals of each of the 5 tissue types in every 4 sequences and obtained the comparative signal summarizing features by calculating them. Additionally, we used the region properties function of the scikit_learn package of Python programming language to find the center of gravity and the major orientation axis of the mass. In this way, we obtained 666 attributes. After eliminating low variance and redundant features, high variance, and non-redundant domain knowledge-inspired features were

retained. After preparing the dimensionality-reduced and cleaned data set described in the previous paragraph, we applied supervised feature selection for each of the datasets using recursive feature elimination (RFE) to obtain the most relevant features (24). Recursive feature elimination is a model-based supervised feature selection method that tests all possible permutations of features and finds the best subset for a given task. The selection is based on the performance scores of many sub-models which test different combinations of features and sort the feature importance scores for the target task. The desired number of highest-ranking features are kept and the remaining are discarded in this feature selection method.

Model Building and Selection:

Support vector machines (SVM) and Random Forest (RF) are two successful classifiers that were commonly used in medical image analysis literature (25,26). The class imbalance problem was high in our dataset which can hamper the predictive ability of our models. Therefore, we implemented 2 strategies to combat with data imbalance problem. The first one was the class_balance method implemented in Random Forest and SVM itself, and the second one was the synthetic minority oversampling technique (SMOTE) which can create synthetic data points for the minority class (27).

Since the number of data points was low, we employed a cross-validation algorithm for training the models and applied the feature standardization, feature selection, and model training together in a nested cross-validation scheme so that there was no data leakage (28). 10 times 5-fold cross-validation training scheme was used to better estimate the skill of built models.

Statistical Analyses

Python scripting language with a scikit-learn package was used for statistical analysis. We reported the f1 scores of all models as mean and standard deviation and the Receiver operating curve area under curve (ROC_AUC) and accuracy values of the most successful model. The overall workflow is summarized in Figure 3.

RESULTS

Of the 101 included patients 80 were IDH mutant (80%) and 21 were IDH wild type (20%).

In the domain knowledge-guided dataset, selected final features were presented in Table 1. Starting from 666 features, 639 remained after variance thresholding and 140 remained after redundancy elimination. Finally, 6 features were selected after supervised feature selection by Recursive Feature Elimination (RFE). One of these features was FLAIR and 4 of them were T1CE based. FLAIR sequence-based selected feature was the ratio of the minimum value of the signal in the necrosis region to that of the minimum signal in the peritumoral normal-appearing brain. 3 of the 4 T1CE-derived selected features were ratios of the maximum, minimum, and standard deviation of the signals of the necrotic region to enhance tumor region. The last T1CE-derived selected feature was the ratio of the standard deviation of the whole tumor region to that of the normal-appearing brain. The last selected feature for the domain knowledge-guided dataset was a spatial feature which was the ratio of volumes of necrotic region to edema region.

In the radiomics dataset, RFE selected final features were presented in Table 1. Starting from 7308 features, we obtained 6 high variance nonredundant relevant features after the application of the same unsupervised and supervised feature selection steps. Two of these features were FLAIR derived one with tumor core and wavelet transformed image and one with whole tumor region and LoG transformed images. Both were second-order features. The third selected feature was 90. Percentile of the histogram of the original image in T1CE sequence with tumor core mask. Remaining three features were T2 sequence-based second-order features.

The combined dataset was constructed by combining radiomics and domain knowledge-based features dataset and subsequent application of the same unsupervised and supervised feature selection. 2 signals, 1 spatial, and 2 radiomics-based features were selected. Selected signal and radiomics features were T2 and FLAIR based with varying contributions of tumor core and whole tumor regions. The selected features are presented in Table 1.

Table 1: Distribution of selected features

	MRI sequence	Tissue mask	Feature type	Feature name
Radiologist inspired and Radiomics Combined	T2	Whole tumor	Signal	Mean ratio
	FLAIR	Whole tumor	Signal	Std ratio
	T2/FLAIR	Enhancing/Core	Signal	Std ratio
	General	Necrosis	Spatial	Volume
	FLAIR LoG sigma=5	Whole tumor	GLSZM 2nd order	Large Area Low Gray Emphasis
	FLAIR Wavelet HLL	Tumor core	First order	Minimum
Radiomics	FLAIR Wavelet LLH	Tumor core	GLRLM 2nd order	Run Entropy
	T1CE Original	Tumor core	First order	90. percentile
	T2 Wavelet LHH	Tumor core	GLCM 2nd order	Cluster Shade
	T2 Original	Whole tumor	GLSZM 2nd order	Zone entropy
	FLAIR Wavelet HLL	Tumor core	First order	Minimum
	FLAIR LoG sigma=5	Whole tumor	GLSZM 2nd order	Large Area Low Gray Emphasis

FLAIR: Fluid Attenuated Inversion Recovery, LoG: Laplace of Gaussian, Wavelet HLL: Wavelet High Low Low, T1CE: T1 contrast enhanced, LHH: Low High High, LLL: Low low low, GLSZM: Gray Level Size Zone Matrix, GLRLM: Gray Level Run Length Matrix, GLCM: Gray Level Co-occurance matrix

Table 2: Performance metrics

		SVM	SVM_SMOTE	SVM_classwg	RF	RF_SMOTE
Radiologist knowledge Inspired	**F1**	0.77, 0.14	0.89, 0.05	0.76, 0.10	0.68, 0.18	0.92, 0.04
	Acc	0.91, 0.05	0.89, 0.04	0.87, 0.06	0.86, 0.04	0.92, 0.04
	AUC	0.89, 0.04	0.97, 0.04	0.95, 0.08	0.85, 0.06	0.96, 0.06
Radiomics	**F1**	0.64, 0.14	0.88, 0.04	0.64, 0.11	0.61, 0.16	0.90, 0.04
	Acc	0.86, 0.05	0.88, 0.04	0.81, 0.06	0.82, 0.04	0.89, 0.05
	AUC	0.92, 0.08	0.94, 0.04	0.91, 0.07	0.83, 0.08	0.96, 0.06
Combined	**F1**	0.84, 0.10	0.93, 0.03	0.81, 0.09	0.70, 0.21	0.93, 0.03
	Acc	0.93, 0.04	0.93, 0.03	0.91, 0.04	0.91, 0.05	0.94, 0.04
	AUC	0.96, 0.06	0.98, 0.02	0.96, 0.06	0.93, 0.07	0.98, 0.02

Acc: Accuracy, AUC: Area Under Curve, SVM: Support Vector Machine, SVM_SMOTE: Support Vector Machine with Syntheric Minority Oversampling Technique, SVM_classwg: Support Vector Machine with class weighting, RF: Random Forest RF_SMOTE: Random Forest with Synthetic Minority Oversampling Technique

Best best-performing model with domain knowledge-based features was Random Forest with SMOTE which achieved a 0.92 f1 score. SVM without SMOTE reached 0.77 and with SMOTE reached 0.89 f1 scores indicating the importance of data balancing strategies in imbalanced dataset conditions.

For the radiomics-based features RF with SMOTE had the best performance with a 0.90 f1 score followed by SVM with SMOTE with a 0.88 f1 score.

On the other hand, combined feature set yielded the best scores. With this strategy, both RF and SVM models achieved similar performance with a 0.93 f1 score whereas SVM without SMOTE yielded still a good score of 0.84 f1 score. The performance metrics of the built models were provided in Table 2 (Table 2) and bar plots in Figure 4.

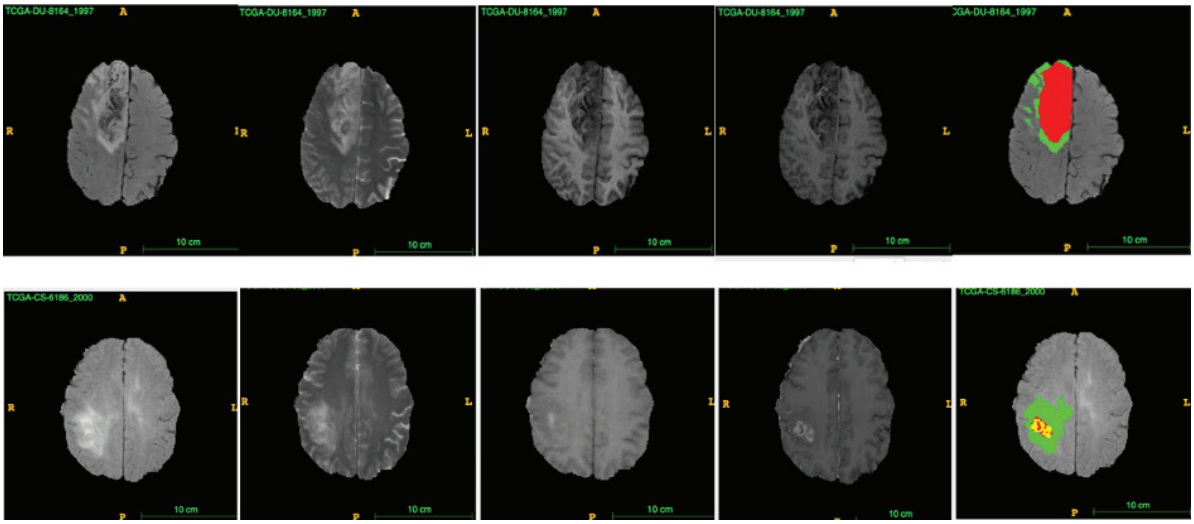

Figure 1: Sample images from IDH dataset. Upper row IDH mutated; lower row IDH wild.
a) FLAIR b) T2 c) T1 d) T1 post contrast e) Segmentation mask overlay
(Red: Necrosis, Yellow: Tumor, Green: Peritumoral edema).
IDH: Isocitrate dehydrogenase

DISCUSSION AND CONCLUSION

The major finding of this study was radiomics-based multiparametric multihabitat features enriched with domain knowledge guided features and reduced to a minimal subset by extensive usage of feature selection methods allowed for better predictive performance than the literature for prediction of IDH status of glial tumors in MRI. The multiregional multisequence model outperformed all other models when radiologist knowledge-based features were integrated. Some recent studies showed local distinct heterogeneous subregions in gliomas (9,10). However, few studies acknowledged this regional heterogeneity in their research plan (29,30). Additionally, multiparametric assessments that leverage the information gained from different sequences are also few (31). Additionally, we explored the value of integration of automatized information gained from human reader assessment approach. To the best of our knowledge, there is no study exploring a multihabitat, multiparametric radiomics model leveraged with automized vectorized human knowledge integrated into the predictive model. Some studies did not consider the curse of dimensionality, a basic data science principle that dictates the total number of predictive features should be a fraction of a total number of samples which may otherwise hamper

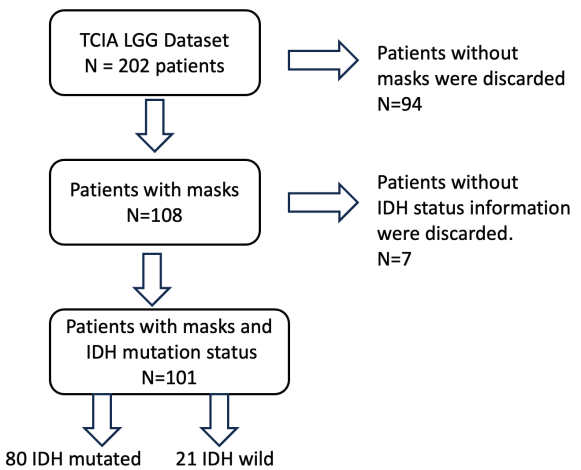

Figure 2: Patient selection process.
TCIA: The cancer imaging Archive. LGG: Low grade Glioma N: Number

their generalizing capacity (31,32). Recalling taking care of this limitation which can lead to overfitting, the above studies exhibited the mean area under a curve of 0.79 to 0.92. Our 6-feature combined model achieved a higher AUC (0.94). The accuracy of this model was 0.93. Our initial feature set for the combined features dataset comprised 7974 features, including 1218 features from each of T1CE, T2, and FLAIR-based tumor core and whole tumor-based region of interests and 666 domain knowledge-based features. This rich comprehensive feature set effectively characterized the tu-

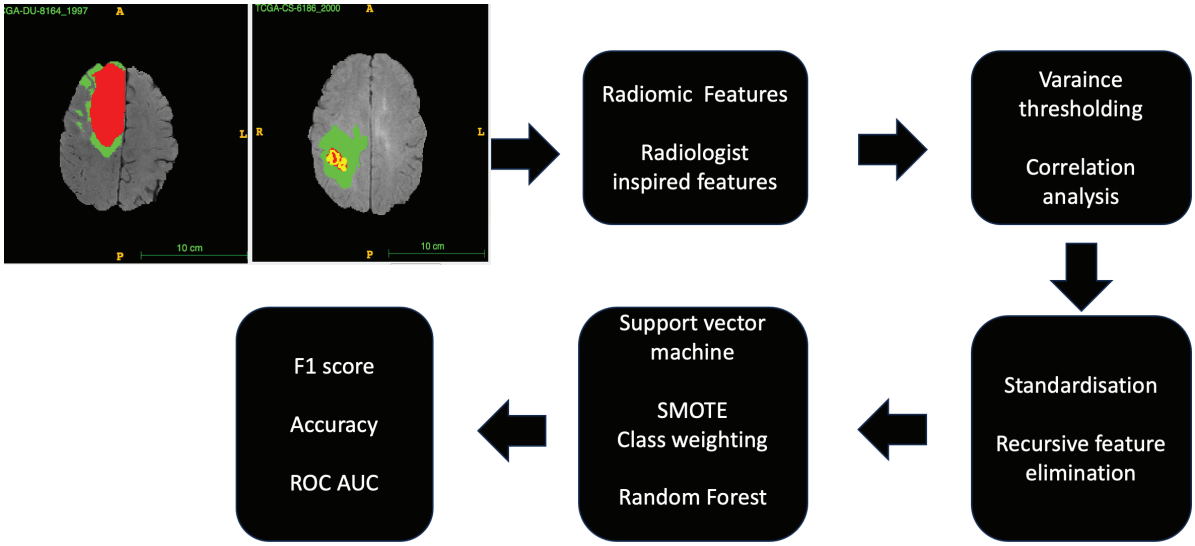

Figure 3: Overall workflow. Three MRI sequences and two tissue masks were given to the system. After radiomic and domain knowledge-based feature extraction, robust, non-redundant, relevant features were selected, followed by model training coupled with imbalance data combatting strategies.
SMOTE: Synthetic Minority Oversampling Technique, ROC_AUC: Receiver Operating Characteristic Area Under Curve

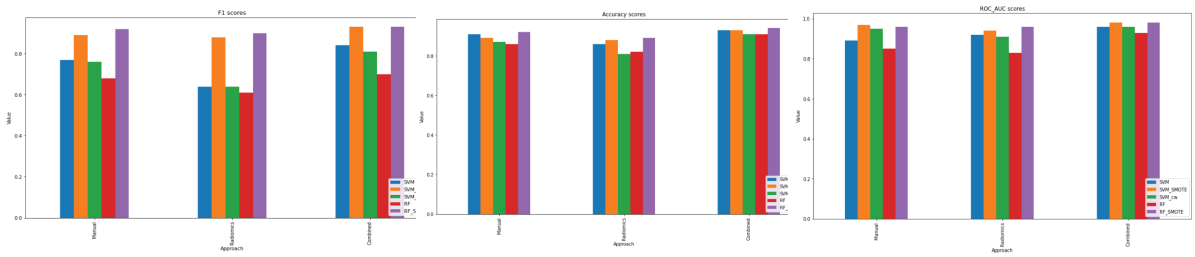

Figure 4: Bar plots of performance metrics.
SVM: Support Vector Machine SVM_SMOTE: Support Vector Machine with Synthetic Minority Oversampling SVM_cw: Support Vector Machine with class weighting RF: Random Forest RF_SMOTE: Random Forest with Synthetic Minority Oversampling Technique

mors. Unsupervised and supervised feature selection methods each having different strengths applied to this feature set reduced the radiomics feature set effectively. Features from different MRI sequence tissue habitat combinations along with domain knowledge-guided features provided a more comprehensive feature set. TCIA data was collected from 5 centers and exhibited considerable variability. We resampled the images into 1 mm resolution, and 0-1 intensity range to obtain spatial and signal normalization. To combat with imbalance dataset problem, we applied class weighting and SMOTE. These steps along with optimized feature extraction and selection strategy improved the predictive ability of our model.

Our results show that among all regions tumor core and whole tumor equally contributed to radiomics relevant features, emphasizing the importance of the multihabitat approach while for the multiparametric options T2 sequence contributed more. Nevertheless, the contribution from T1CE and FLAIR sequences could not be neglected as well as a contribution from signal and spatial-based features. This observation indicated that the imaging phenotypes within distinct tumor subregions and from different MRI sequences may contribute differently to the outcome. In ref. (33) The authors demonstrated that tumor heterogeneity is not limited to the tumor core but also involves the edema area. In ref. (34) The authors have shown

that radiomics features from the peritumoral edema area could predict survival better than from enhancing tumor and necrosis areas. The authors in ref. (35) showed that a higher ratio of non-enhancing areas is associated with IDH1 mutation in HGG. Similarly in our study, necrosis volume, and signal of the peritumoral region in T2 and FLAIR had high coefficients.

Glial tumors harboring IDH mutation accumulate 2-hydroxyglutarate within the tumor that can be identified by MR spectroscopy which is a promising technique to detect IDH mutation noninvasively in glial tumors (33). Another promising modality is T2 perfusion imaging which showed that IDH mutant gliomas tend to present lower regional cerebral blood volume than wild counterparts (36). Nevertheless, these techniques are advanced and cannot be used outside specialized centers (37,38). On the other hand, our algorithm has broader applicability due to the advantage that it is based on routinely acquired standard protocols. The readily availability of the system operating on standard sequences could help better clinical adoption of our model. This may help the clinician in decision-making process for further evaluation or taking actions for intervention. Providing that our results are validated on large cohorts, our model might reduce the interventions for determination of IDH subtype, the morbidity to the patient based on additional operations, the business of neurosurgery departments, and the overall cost to the healthcare system. This might have additional positive effects on the society.

The most important limitation of our dataset was that it was a public dataset so we could not explore clinical variables besides imaging features. Another limitation was the small sample size. Finally, as most of the radiomics studies feature stability over external validation sets was an important issue that should be tested in large cohorts.

In conclusion, the IDH mutation phenotype of glial tumors can be predicted by a combination of human radiologist-imitated features and multiparametric multihabitat radiomics features.

Conflict-of-interest and financial disclosure

The authors declare that they have no conflict of interest to disclose. The authors also declare that they did not receive any financial support for the study.

REFERENCES

1. Bakas S, Akbari H, Sotiras A, et al. Advancing The Cancer Genome Atlas glioma MRI collections with expert segmentation labels and radiomic features. Sci Data. 2017;4:170117.
2. Parsons DW, Jones S, Zhang X, et al. An Integrated Genomic Analysis of Human Glioblastoma Multiforme. Science. 2008;321:1807-12.
3. Eckel-Passow JE, Lachance DH, Molinaro AM, et al. Glioma Groups Based on 1p/19q, IDH, and TERT Promoter Mutations in Tumors. N Engl J Med. 2015;372:2499-508.
4. Hartmann C, Hentschel B, Wick W, et al. Patients with IDH1 wild type anaplastic astrocytomas exhibit worse prognosis than IDH1-mutated glioblastomas, and IDH1 mutation status accounts for the unfavorable prognostic effect of higher age: implications for classification of gliomas. Acta Neuropathol. 2010;120:707-18.
5. Louis DN, Perry A, Reifenberger G, et al. The 2016 World Health Organization Classification of Tumors of the Central Nervous System: a summary. Acta Neuropathol. 2016;131:803-20.
6. Berger TR, Wen PY, Lang-Orsini M, Chukwueke UN. World Health Organization 2021 Classification of Central Nervous System Tumors and Implications for Therapy for Adult-Type Gliomas: A Review. JAMA Oncol. 2022;8(10):1493-501.
7. van Kempen EJ, Post M, Mannil M, et al. Accuracy of Machine Learning Algorithms for the Classification of Molecular Features of Gliomas on MRI: A Systematic Literature Review and Meta-Analysis. Cancers (Basel). 2021;13(11):2606.
8. Yang H, Ye D, Guan K-L, Xiong Y. IDH1 and IDH2 Mutations in Tumorigenesis: Mechanistic Insights and Clinical Perspectives. Clin Cancer Res. 2012;18:5562-71.
9. Sottoriva A, Spiteri I, Piccirillo SG, et al. Intratumor heterogeneity in human glioblastoma reflects cancer evolutionary dynamics. Proc Natl Acad Sci. 2013;110:4009-14.
10. Patel AP, Tirosh I, Trombetta JJ, et al. Single-cell RNA-seq highlights intratumoral heterogeneity in primary glioblastoma. Science. 2014;344:1396-401.
11. Molenaar RJ, Botman D, Smits MA, et al. Radioprotection of IDH1-Mutated Cancer Cells by the IDH1-Mutant Inhibitor AGI-5198. Cancer Res. 2015;75:4790-802.
12. Patel SH, Poisson LM, Brat DJ, et al. T2–FLAIR Mismatch, an Imaging Biomarker for IDH and 1p/19q Status in Lower-grade Gliomas: A TCGA/TCIA Project. Clin Cancer Res. 2017;23(20):6078-85.
13. Parmar C, Grossmann P, Bussink J, Lambin P, Aerts

HJWL. Radiomic feature robustness and reproducibility in volumetric radiomic analysis. Sci Rep. 2015;5:13087.
14. Chang K, Bai HX, Zhou H, et al. Residual Convolutional Neural Network for the Determination of IDH Status in Low- and High-Grade Gliomas from MR Imaging. Clin Cancer Res. 2018;24(5):1073-81.
15. Zhou H, Vallières M, Bai HX, et al. MRI features predict survival and molecular markers in diffuse lower-grade gliomas. Neuro Oncol. 2017;19(6):862-70.
16. VASARI Research Project. [homepage on the Internet]. https://wiki.cancerimagingarchive.net/display/Public/VASARI+Research+Project. Accessed June 21, 2018.
17. Julesz B, Gilbert EN, Shepp LA, Frisch HL. Inability of Humans to Discriminate between Visual Textures That Agree in Second Order Statistics Revisited. Perception. 1973;2(4):391-405.
18. Lambin P, Leijenaar RT, Deist TM, et al. Radiomics: the bridge between medical imaging and personalized medicine. Nat Rev Clin Oncol. 2017;14:749-62.
19. Smits M, van den Bent MJ. Imaging Correlates of Adult Glioma Genotypes. Radiology. 2017;284:316-31.
20. Hu LS, Eschbacher JM, Heiserman JE, et al. Radiogenomics to characterize regional genetic heterogeneity in glioblastoma. Neuro Oncol. 2017;19(1):128-37.
21. Zhang B, Tian Q, Wang L, et al. Radiomics strategy for molecular subtype stratification of lower-grade glioma: detecting IDH and TP53 mutations based on multimodal MRI. J Magn Reson Imaging. 2018;48:916-26.
22. Li ZC, Bai H, Sun Q, et al. Multiregional radiomics profiling from multiparametric MRI: Identifying an imaging predictor of IDH1 mutation status in glioblastoma. Cancer Med. 2018;7(12):5999-6009.
23. Zhang B, Chang K, Ramkissoon S, et al. Multimodal MRI features predict isocitrate dehydrogenase genotype in high-grade gliomas. Neuro Oncol. 2017;19(1):109-17.
24. Yu J, Shi Z, Lian Y, et al. Noninvasive IDH1 mutation estimation based on a quantitative radiomics approach for grade II glioma. Eur Radiol. 2017;27(8):3509-22.
25. Andronesi OC, Rapalino O, Gerstner E, et al. Detection of oncogenic IDH1 mutations using magnetic resonance spectroscopy of 2-hydroxyglutarate. J Clin Invest. 2013;123(9):3659-63.
26. Lee S, Choi SH, Ryoo I, et al. Evaluation of the microenvironmental heterogeneity in high-grade gliomas with IDH1/2 gene mutation using histogram analysis of diffusion-weighted imaging and dynamic-susceptibility contrast perfusion imaging. J Neurooncol. 2015;121(1):141-50.
27. Yamashita K, Hiwatashi A, Togao O, et al. MR Imaging-Based Analysis of Glioblastoma Multiforme: Estimation of IDH1 Mutation Status. AJNR Am J Neuroradiol. 2016;37(1):58-65.
28. Kickingereder P, Sahm F, Radbruch A, et al. IDH mutation status is associated with a distinct hypoxia/angiogenesis transcriptome signature which is non-invasively predictable with rCBV imaging in human glioma. Sci Rep. 2015;5:16238.
29. Zhao J, Huang Y, Song Y, et al. Diagnostic accuracy and potential covariates for machine learning to identify IDH mutations in glioma patients: evidence from a meta-analysis. Eur Radiol. 2020;30(8):4664-74.
30. Choi Y, Nam Y, Lee YS, et al. IDH1 mutation prediction using MR-based radiomics in glioblastoma: comparison between manual and fully automated deep learning-based approach of tumor segmentation. Eur J Radiol. 2020;128:109031.
31. Cortes C, Vapnik V. Support-vector networks. Mach Learn. 1995;20(3):273-97.
32. Ho TK. Random decision forests. In: Proceedings of 3rd international conference on document analysis and recognition. 1995. p. 278-282.
33. Chawla NV, Bowyer KW, Hall LO, Kegelmeyer WP. Smote: synthetic minority over-sampling technique. J Artif Intell Res. 2002;16:321-57.
34. Chandrashekar G, Sahin F. A survey on feature selection methods. Comput Electr Eng. 2013;40(1):16-28.
35. Kumar V, Minz S. Feature Selection: A literature review. Smart Comput Rev. 2014;4(3):211-29.